analytical chemistry

Article

Cite This: *Anal. Chem.* 2018, 90, 11393−11400

pubs.acs.org/ac

Bifunctional Super-resolution Imaging Probe with Acidity-Independent Lysosome-Retention Mechanism

Zhongwei Xue,[†] Siyu Wang,[†] Jian Li,[†] Xin Chen,*[,‡] Jiahuai Han,[‡] and Shoufa Han*[,†]

[†]Department of Chemical Biology, College of Chemistry and Chemical Engineering, State Key Laboratory for Physical Chemistry of Solid Surfaces, the Key Laboratory for Chemical Biology of Fujian Province, The MOE Key Laboratory of Spectrochemical Analysis & Instrumentation, and Innovation Center for Cell Signaling Network, Xiamen University, Xiamen, 361005, China

[‡]State key Laboratory of Cellular Stress Biology, Innovation Center for Cell Signaling Network, School of Life Sciences, Xiamen University, Xiamen, 361005, China

Supporting Information

ABSTRACT: Spatiotemporal imaging is of enormous use to explore organelle biology, necessitating organelle-tracing techniques reliable in varied cell stress. We herein reported lysosomal imaging using rhodamine-X-integrated sialic acid (^{ROX}SA), which is stably maintained in lysosomes irrespective of lysosomal pH changes. Exhibiting bright fluorescence and superior photostability, ^{ROX}SA enables 120 h continual tracking of fusion/fission of lysosomes and mitochondrion−lysosome interaction in mitophagy. Relative to conventional acidotropic probes prone to dissipation from stressed lysosomes, ^{ROX}SA offers a new route for long-term tracking of stressed lysosomes relevant to diverse pathological conditions.

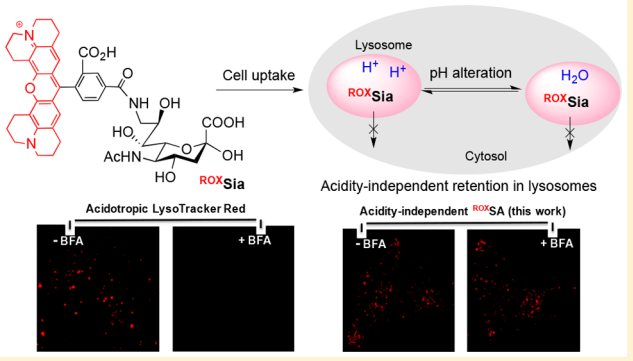

Organelles are a set of membrane-bound cellular subunits with distinct biological functions. Organelle stress and associated organelle interplay are crucial for cell performance, as evidenced by lysosomal−mitochondrial cross-talk in cell death and cell metabolism.[1] Lysosomes are acidic organelles vital to cell events ranging from immunity and cell homeostasis to cell death.[2] Stressed lysosomes are manifested in several pathological conditions.[3] For example, lysosomal pH is elevated in cell aging and lysosomal storage diseases,[4] while lysosome positioning is markedly altered in nutrient deficiency.[5] Lysosomal degradation of impaired organelles is essential for cell health, and the defect in mitochondrial turnover (mitophagy) is implicated in myriad pathological events such as Parkinson's diseases.[6]

Lysosomes are routinely imaged with acidotropic dyes that are protonated in acidic medium and thus accumulate in lysosomes driven by lysosomal acidity.[7] Albeit widely used, these probes are prone to dissipate from lysosomes upon lysosomal pH elevation owing to loss of probe protonation or extended cell culturing,[5] which compromises the staining or tracking of stressed lysosomes in cell signaling events or diseased cells. For instance, a rhodamine−lactam-based pH sensor suffers from significant signal loss from stressed lysosomes in cell death.[7a] Super-resolution microscopy has overcome the diffraction limit of conventional light microscopy, allowing resolution down to ∼10 nm to be achieved.[8] Super-resolution imaging is of enormous use in investigating cell events,.[9] However, classical probes of lysosomes are prone to photobleaching[10] and thus compromise their use in super-resolution imaging. In view of these limitations, imaging agents with superior photostability, yet allowing spatiotemporal tracking of stressed lysosomes irrespective of lysosomal pH changes, would be of significance for probing the roles of lysosomes and lysosome−mitochondrion interplay in biology and diseases.

Sialic acid (SA) is a monosaccharide that could be uptaken from an extracellular milieu into lysosomes in mammalian cells. Herein we reported that rhodamine-X conjugated at C9 of SA (^{ROX}SA), with superior photostability, selectively stains lysosomes and is trapped in lysosomes irrespective of the alterations of lysosomal pH. These advantages enable whole course tracking of lysosome dynamics and lysosome−mitochondrion interaction in mitophagy.

EXPERIMENTAL PROCEDURE

Materials and Methods. Baflomycin A1 (BFA) was purchased from Selleck. LysoTracker Red and MitoTracker Green were obtained from Thermo Fisher. Mouse embryonic fibroblasts were collected from embryos from C57BL6/J mice at dpc 12.5, and all other cell lines were obtained from American Type Culture Collection (ATCC). Transient transfection of HEK293T cells was performed using a calcium phosphate method. Lentiviral infection was used for stable expression. Recombinant lentiviruses were packaged in 293T cells in the presence of helper plasmids (pMDLg, pRSV-REWV and pVSV-G)

Received: May 28, 2018
Accepted: August 27, 2018
Published: August 27, 2018

DOI: 10.1021/acs.analchem.8b02365
Anal. Chem. 2018, 90, 11393−11400

using a calcium phosphate precipitation method. The transfected cells were cultured for 48 h and the viruses were collected for infection. All cells were maintained in Dulbecco's modified Eagle's medium (DMEM), supplemented with 10% fetal bovine serum, 2 mM L-glutamine, 100 IU penicillin, and 100 mg/mL streptomycin at 37 °C in a humidified incubator under 5% CO_2. Full-length cDNA of Lamp2 was cloned into *Bam*HI and XhoI sites of the lentiviral vector pBOB-GFP using the Exo III-assisted ligase-free cloning method.[11] All plasmids were verified by DNA sequencing. For lentivirus production, HEK293T cells were transfected by the calcium phosphate precipitation method. The virus-containing medium was harvested 36−48 h later and was added to cells of interest.

The fluorescence spectra were performed on a SpectraMax M5 instrument. Confocal fluorescence microscopic imaging was performed on a Zeiss LSM 780 apparatus using the following filters: λ_{ex} = 488 nm and λ_{em} = 499−553 nm for GFP and MitoTracker green; λ_{ex} = 565 nm and λ_{em} = 585−733 nm for rhodamine and LysoTracker Red. The fluorescence of ROX and Lysotracker Red in cells was respectively shown in red in the figures while fluorescence of GFP and MitoTracker Green was shown in green. Images of merged fluorescence were processed using Photoshop CS6. Quantitative imaging analysis was carried out on unprocessed images using ImageJ software. A graph was generated by GraphPad Prism5 and origin 8.0 software. Flow cytometry was performed on BD Fortessa equipment; the fluorescence emission of ROX was recorded using an FL2 filter (590−630 nm) and λ_{ex} of 561 nm. Under identical conditions, 10000 cells were gated and analyzed. The data were processed by GraphPad Prism5. Stochastic optical reconstruction microscopy (STORM) imaging was performed on an N-STORM microscope (Nikon Instruments) according to published procedures.[12]

Synthesis of ^{ROX}SA. 5-ROX (1.3 g, 2.4 mmol) was dissolved in anhydrous *N*,*N*-dimethylformamide (DMF, 10 mL) followed by addition of triethylamine (266 mg, 2.6 mmol) and HATU (957 mg, 2.5 mmol) under N_2 atmosphere. The mixture was stirred at room temperature for 1 h followed by addition of compound **A** (773 mg, 2.4 mmol). The solution was stirred 2 h at room temperature and then evaporated to remove the solvent. The residue was purified by silica gel column chromatography using DCM/MeOH/TEA (100:10:1, v/v/v) as the eluent to give a deep red solid which was dissolved in aqueous methanol (10 mL) containing sodium hydroxide (1 M). The mixture was stirred and monitored by TLC until the hydrolysis was complete. The mixture was neutralized with Amberlite IR120-acid form ion-exchange resin, filtered, and evaporated. The residue was purified by silica gel column chromatography using DCM/MeOH/TEA (25:50:1, v/v/v) as the eluent to give ^{ROX}SA (675 mg) in 32% overall yield. ^{1}H NMR (500 MHz, CD_3OD): δ 8.49 (s, 1 H), 8.01 (d, J = 6.9 Hz, 1 H), 7.29 (d, J = 4.7 Hz, 1 H), 6.78 (s, 2 H), 4.12 (d, J = 9.4 Hz, 1 H), 4.03 (t, J = 9.2 Hz, 2 H), 3.91 (d, J = 9.1 Hz, 1 H), 3.90−3.84 (m, 1 H), 3.59−3.43 (m, 10 H), 3.07 (t, J = 6.0 Hz, 4 H), 2.78−2.62 (m, 4 H), 2.16−2.06 (m, 5 H), 2.01 (s, 3 H), 1.99−1.89 (m, 5 H). ^{13}C NMR (214 MHz, CD_3OD): δ 176.18, 173.02, 171.37, 168.00, 158.04, 152.08, 150.83, 140.86, 135.44, 129.68, 128.50, 127.72, 126.38, 123.45, 112.73, 104.93, 70.52, 67.47, 52.95, 50.42, 49.95, 33.91, 27.20, 21.69, 20.48, 19.66, 19.59, 13.42. HRMS ($C_{44}H_{49}N_4O_{12}^+$): calcd (M^+), 825.3341; found, 825.3350.

Staining of Lysosomes with ^{ROX}SA. Lamp2-GFP$^+$ HeLa cells were incubated in DMEM with ^{ROX}SA (25 μM) for 16 h and then analyzed by confocal fluorescence microscopy. In parallel, HeLa, A549, 293, CHO, L929, and MEF cells were incubated in DMEM supplemented with ^{ROX}SA (25 μM) for 16 h and then stained with LysoTracker Green DND26 (1 μM) for 30 min. The cells were washed with PBS and then analyzed by confocal fluorescence microscopy.

Incapability of ROX and 5-ROX To Stain Lysosomes. HeLa cells were stained with ROX (5 μM, 1 h) or 5-ROX (5 μM, 1 h) in the presence of LysoTracker Green (1 μM, 30 min) and then imaged by confocal fluorescence microscopy.

Lysosomal Membrane Integrity-Dependent Lysosome Staining with ^{ROX}SA. GFP-Lamp2$^+$ HeLa cells were incubated in DMEM supplemented with 25 μM ^{ROX}SA for 16 h, and further treated with no addition, BFA (100 nM), or chloroquine (100 μM) in DMEM for 0, 6, and 12 h. The cells were analyzed by flow cytometry.

Lysosomal Acidity-Independent Retention of ^{ROX}SA. HeLa cells were incubated in ^{ROX}SA (25 μM) in DMEM for 16 h and then incubated in DMEM spiked with or without BFA (100 nM) for 8 h. For the control, HeLa cells were incubated in LysoTracker Red (1 μM) in DMEM for 30 min and then incubated in DMEM spiked with or without BFA (100 nM) for 8 h. The cells were analyzed by confocal fluorescence microscopy.

pH Titration of ^{ROX}Sia. ^{ROX}Sia was added to sodium phosphate buffer containing 30% DMF (pH: 3.5, 4.0, 4.5, 5.0, 5.5, 6.0, 6.5, 7.0, 7.5, 8.0, and 8.5) to a final concentration of 10 μM. Fluorescence emisison spectra were recorded using λex = 585 nm for ROX, and the fluorescence emission at 615 nm was plotted over buffer pH.

Probing the Mechanisms of Lysosomal Uptake of ^{ROX}SA. HeLa cells were incubated with ^{ROX}SA (25 μM) for 16 h in DMEM spiked with 5-(N-ethyl-*N*-isopropyl)amiloride (EIPA, 50 μM), chlorpromazine (CPZ, 5 μM), or Filipin III (2 μM). The cells were washed and analyzed by confocal fluorescence microscopy.

Dependence of ^{ROX}SA Uptake on Lysosomal Acidity. HeLa cells were stained by ^{ROX}SA (50 μM) with or without BFA (20 nM) in DMEM for 16 h. The cells were analyzed by confocal fluorescence microscopy.

Cytotoxicity of ^{ROX}SA. L929 and HeLa cells were cultured in a 48-well cell culture plate with DMEM containing ^{ROX}SA (0, 5, 10, 25, and 50 μM) for 0−48 h. The cell number and cell viability were determined by MTT assay. MEF primary cells were incubated with ^{ROX}SA (25 μM), Staurosporine (apoptosis inducer, 1 μM), or no addition for 24 h, and then incubated with SYTOX-green (25 nM) for 30 min to stained cells. The cells were washed with DMEM, maintained in fresh DMEM for 24 h, and then imaged by confocal fluorescence microscopy.

Retention of ^{ROX}SA in Lysosomes in Mitophagy. U2OS cells were cultured in DMEM spiked with ^{ROX}SA (25 μM, 16 h)/MitoTracker Green (1 μM, 30 min) or LysoTracker Red (1 μM, 30 min)/MitoTracker Green (1 μM, 30 min). The cells were washed with DMEM and then maintained in DMEM depleting serum. Cells were analyzed at 0 or 24 h by confocal microscopy. The cells after 24 h starvation were further maintained in DMEM containing BFA (100 nM) for 8 h and then imaged by confocal microscopy. U2OS cells were cultured in DMEM spiked with ^{ROX}SA (25 μM) for 16 h and then starved for 0, 24, 48, and 72 h and analyzed by flow cytometry.

Staining of Overall Lysosomes with ^{ROX}SA in mitophagy. U2OS were cultured in DMEM spiked with ^{ROX}SA (25 μM) for 16 h and then maintained in DMEM

DOI: 10.1021/acs.analchem.8b02365
Anal. Chem. 2018, 90, 11393−11400

Scheme 1. Schematic of Lysosomal Imaging with ^{ROX}SA via Acidity-Independent Probe Retention in Lysosomes

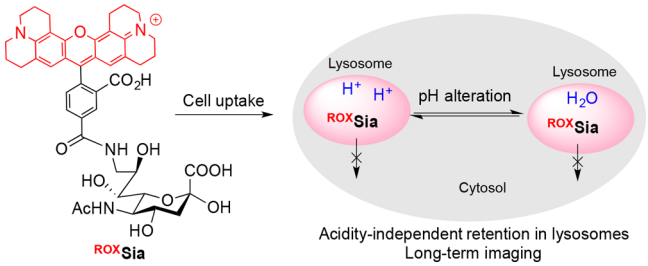

depleting serum to trigger mitophagy. At fixed time intervals during 0−120 h post-starvation, a portion of the cells were stained with LysoTracker Blue (500 nM) for 30 min and then imaged by confocal microscopy for intracellular fluorescence colocalization.

Detecting Lysosome Changes and Lysosomal−Mitochondrial Interactions in Mitophagy. U2OS cells were cultured in DMEM spiked with ^{ROX}SA (5 μM) for 24 h and then further cultivated with MitoTracker Green (5 μM) for 0.5 h. The cells were washed with DMEM and then maintained in DMEM depleting serum to trigger mitophagy. Cells were analyzed at 0−120 h by confocal microscopy. The cells at 24 h post-starvation were consecutively imaged to track lysosomal changes. In separate experiments, time course analyses were performed on the cells at 24 h post-starvation.

Super-resolution Imaging of Lysosomes with ^{ROX}SA. HeLa cells were cultured on an eight-well chambered cover glass (Thermo Fisher) and loaded with ^{ROX}SA or LysoTracker Red. To obtain STORM images, we imaged the sample in the imaging buffer that contained 50 mM Tris (pH 8.0), 10 mM NaCl, 0.5 mg/mL glucose oxidase (Sigma-Aldrich), 40 μg/mL catalase (Sigma-Aldrich), 10% (w/v) glucose, and 143 mM β-mercaptoethanol (Fluka). Cells were illuminated with 561 nm laser excitation, and fluorescence was detected with an iXon DU897 (Andor) EMCCD camera with an exposure time of 16 ms. Typically, 5000−10000 frames were collected, and images were reconstructed using the N-STORM module in NIS-Elements AR software.

RESULTS AND DISCUSSION

Acidity-Independent Imaging of Lysosomes with ^{ROX}SA. Sialin is the protein transporter that exports SA from lysosomes into cytosol, and a defect in sialin function leads to salla diseases hallmarked by SA accumulation in lysosomes.[13] Sia modified with small size substituents such as azide or alkyne have been incorporated into cell surface glycocalyx, and sialin is likely responsible for relocation of these Sia analogues from lysosomes into cytosol.[14] We anticipated that SA bearing appropriate moieties (e.g., bulky/ionic) might impede sialin recognition and thus could be trapped in lysosomes, which in principle could be exploited to achieve acidity-independent imaging of stressed lysosomes (Scheme 1).

^{ROX}SA was synthesized and then incubated with HeLa cells expressing green fluorescence protein-tagged lysosomal membrane associated protein-2 (GFP-Lamp2), a constituent membrane protein of lysosomes. Confocal microscopy revealed

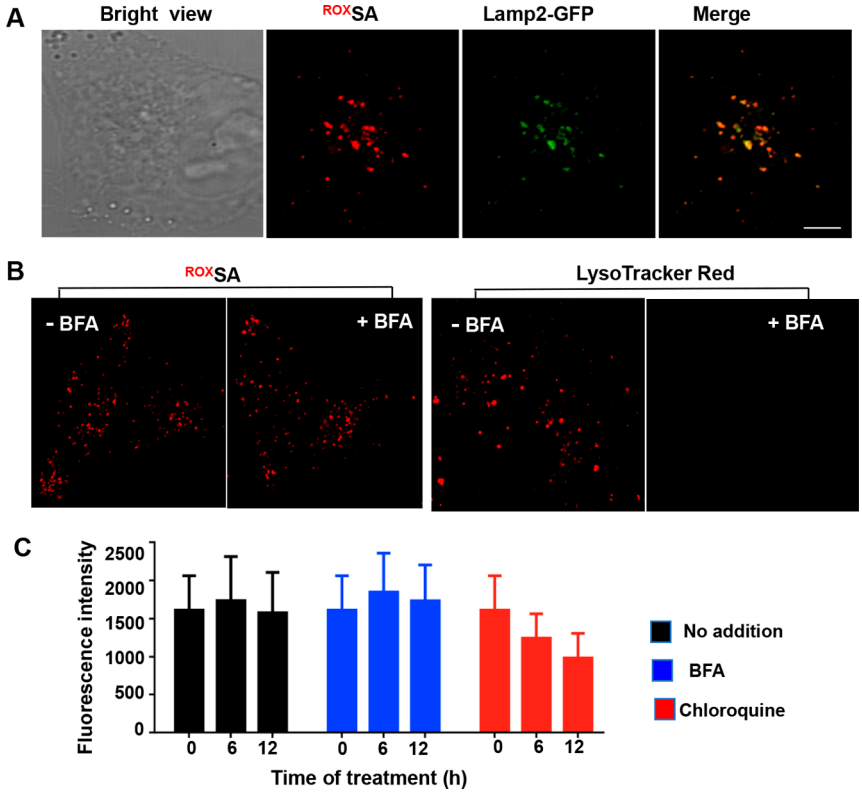

Figure 1. Lysosomal imaging with ^{ROX}SA of acidity-independent retention in lysosomes. (A) ^{ROX}SA colocalizes with GFP-Lamp2^{+} in HeLa cells. (B) Acidity-independent lysosomal retention of ^{ROX}SA. Cells stained with ^{ROX}SA or LysoTracker Red were cultured in medium spiked with or without BFA before confocal microscopy analysis. (C) Dependence of lysosomal membrane integrity on the retention of ^{ROX}SA. ^{ROX}SA-stained cells were treated with BFA, chloroquine, or no addition for varied periods of time (0, 6, and 12 h) and then quantitated by flow cytometry for intracellular fluorescence. Scale bars, 10 μm.

DOI: 10.1021/acs.analchem.8b02365
Anal. Chem. 2018, 90, 11393−11400

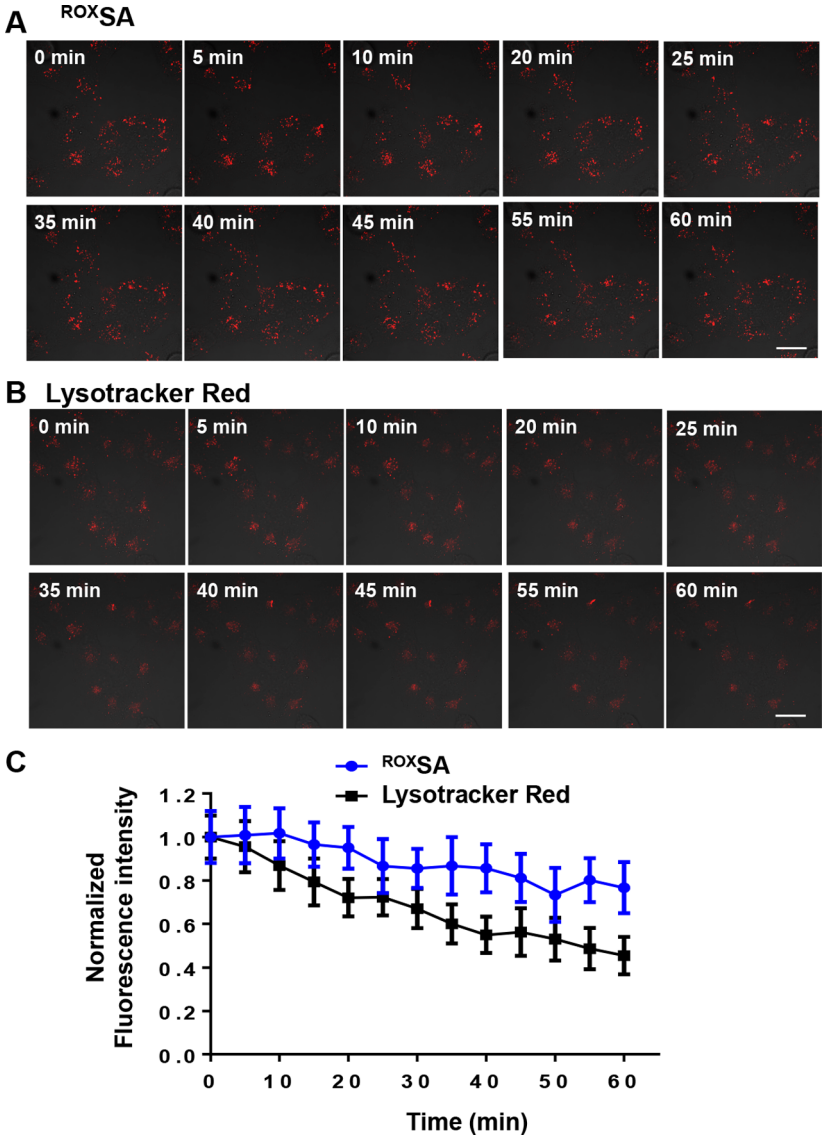

Figure 2. Photostability of ^{ROX}SA. HeLa cells stained with ^{ROX}SA or Lysotracker Red were subjected to constant laser illumination and then analyzed by confocal fluorescence microscopy or flow cytometry at indicated time points (0–60 min). Confocal microscopic images of ^{ROX}SA^{+} cells (A) or Lysotracker Red^{+} cells (B) after illumination. (C) Normalized fluorescence intensity that remained in cells after laser illumination. The intracellualr fluorescence was quantitated by flow cytometry and then normalized as a function of illumination time. Scale bars, 10 μm.

punctate ROX fluorescence colocalized with GFP-Lamp2 (Figure 1A), proving stringent selectivity of ^{ROX}SA for lysosomes. In contrast, no lysosome-specific fluorescence could be observed in cells treated with 5-carboxy-ROX or ROX free of the sugar functionality (Figure S1, Supporting Information), showing the essential role of SA moiety of ^{ROX}SA for lysosome targeting. In addition, ^{ROX}SA effectively stains lysosomes in A549, 293, CHO, HeLa, L929 cells, and primary mouse embryonic fibroblasts (MEFs; Figure S2, Supporting Information), whereby ^{ROX}SA was uncovered to colocalize with LysoTracker Green, a commercial dye specific for lysosomes. These results demonstrate the selectivity of ^{ROX}SA for lysosomes in diverse cell lines. Sugar-labeled profluorophores responsive to acidic pH have been employed for lysosome imaging.[15] Since these profluorophores are nonfluorescent in cytosol (pH 7), the distribution of these glycoprobes between lysosomes and cytosol remains to be determined. In contrast, ^{ROX}SA exhibits pH-independent intense "always-on" fluorescence in the range of pH 4–9 (Figure S3, Supporting Information). The lack of ROX fluorescence in extralysosomal settings validates the selectivity of ^{ROX}SA for lysosomes over cytosol.

To assess the impacts of lysosomal acidity on ^{ROX}SA retention, HeLa cells stained with ^{ROX}SA were further cultivated in fresh medium spiked with Baflomycin A1 (BFA), a potent V-ATPase inhibitor capable of neutralizing lysosomes.[16] Time course analysis revealed discrete and bright ROX signals remained in BFA-treated cells, whereby the intracellular fluorescence remained constant up to 12 h incubation (Figure 1B,C). By contrast, cells stained with LysoTracker Red exhibited complete loss of fluorescence in the presence of BFA (Figure 1B). Collectively, these results validate acidity-independent retention of ^{ROX}SA in lysosomes, which is distinct to acidotropic imaging agents. The acidity-independent probe retention in lysosomes indicates that hydrophilic ^{ROX}SA is restricted from passive diffusion across the lysosomal membrane. To confirm this, HeLa cells stained with ^{ROX}SA were treated with chloroquine to induce lysosomal membrane permeabilization.[17] Relative to control cells, chloroquine-treated cells exhibited

DOI: 10.1021/acs.analchem.8b02365
Anal. Chem. 2018, 90, 11393–11400

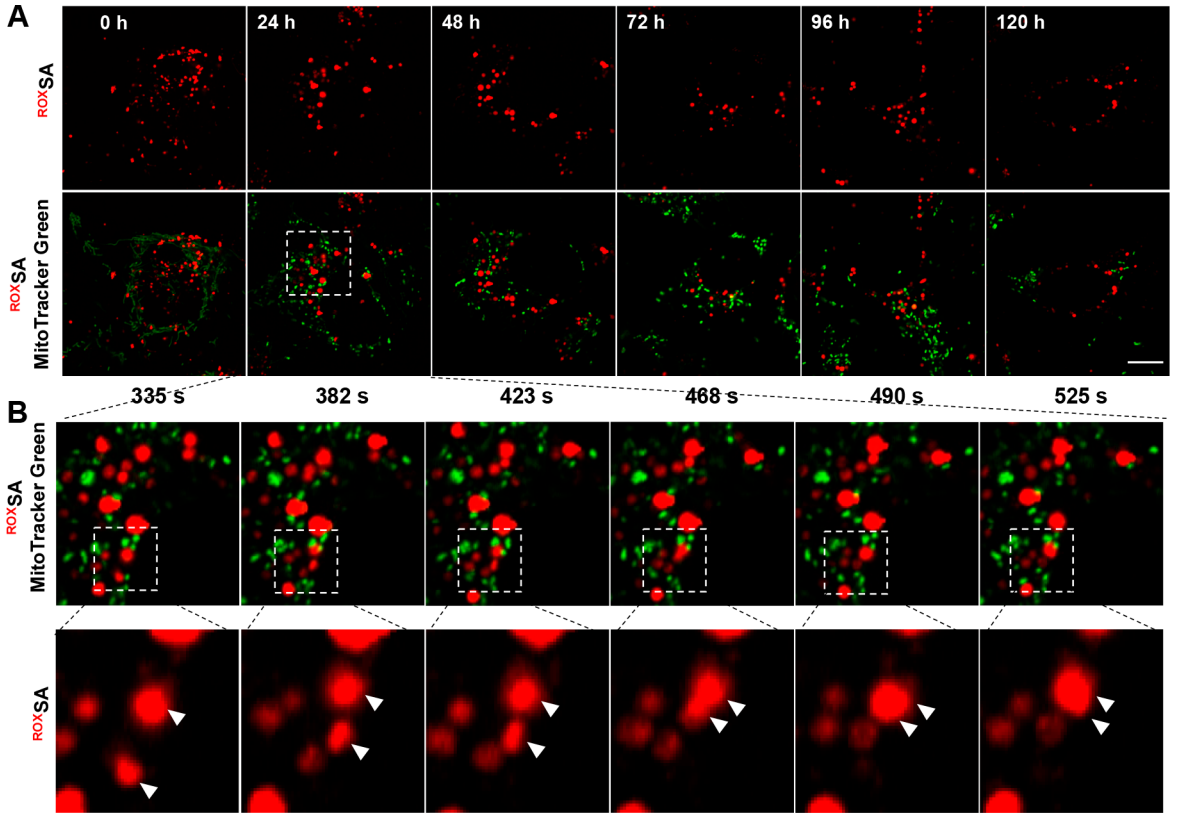

Figure 3. Imaging of dynamic lysosomes in mitophagy with ^{ROX}SA. U2OS cells stained with ^{ROX}SA and MitoTracker Green were starved for 0−120 h in DMEM depleting serum to induce mitophagy. (A) Confocal microscopic images of mitophagic cells at 0−120 h post-starvation. (B) Snapshots of mitophagic cells at 24 h post-starvation. The zoomed images showed the fusion of two individual lysosomes indicated by arrowheads. Scale bar, 10 μm.

gradual loss of ^{ROX}SA over time (Figure 1C), which is ascribed to leakage of ^{ROX}SA from permeabilized lysosomes, showing that the acidity-independent trapping of ^{ROX}SA depends on lysosome membrane integrity.

We then explored the cellular routes responsible for lysosomal accumulation of ^{ROX}SA. Endocytosis often leads to accumulation of exogenous materials into lysosomes. To assess whether a specific endocytosis process contributes to probe uptake. HeLa cells were treated with ^{ROX}SA in the presence of distinct endocytotic inhibitors, including 5-(6N-ethyl-6N-isopropyl)amiloride which inhibits macropinocytosis and phagocytosis,[18] chlorpromazine which is an inhibitor of clathrin-mediated endocytosis,[19] and Filipi III/M-βCD which inhibits lipid raft/caveolae-mediated endocytosis.[20] No inhibitory effect is observed on the levels of ^{ROX}SA in lysosomes by EIPA, CPZ, or Filipi III/M-βCD (Figure S4, Supporting Information), showing that lysosomal uptake of ^{ROX}SA is largely independent of endocytosis. The acidic pH is critical for lysosomal functionality. For instance, ion channels and transporters often rely on the H^+ gradient to transport ions in and out of lysosomes.[21] Hence HeLa cells were treated with BFA and then cultured with ^{ROX}SA. No ^{ROX}SA signals were observed in BFA-treated cells undergoing pH-elevated lysosomes (Figure S5, Supporting Information), suggesting a role of H^+ antiporters in ^{ROX}SA-based lysosomal staining. Relative to zwitterionic ROX moiety, dinitrobenzene (DNP) is neutral and less bulky. DNP-conjugated SA was metabolically incorporated on the cell surface,[22] owing to sialin-mediated export of ^{DNP}SA out of lysosomes into cytosol. The sequestering of ^{ROX}SA in lysosomes indicates that the ROX moiety blocks export of ^{ROX}SA out of lysosomes by sialin. Differing from classical lysosomal probes, hydrophobic and readily diffusing across the cell membrane, ^{ROX}SA is hydrophilic and impermeable to lysosomal membrane and requires extended time periods to stain lysosomes (Figure 1B). Given the aforementioned independence of ^{DNP}SA on endocytosis, ^{ROX}SA is likely mediated by specific H^+ antiporters to stain lysosomes.

Photobleaching often compromised the use of synthetic dyes in bioimaging. Hence HeLa cells stained with ^{ROX}SA or LysoTracker Red were exposed to constant laser illumination whereby ^{ROX}SA maintained higher levels of fluorescence than Lysotracker Green (Figure 2), suggesting the superior photostability of ^{ROX}SA. In addition, no detectable cytotoxicity was noticed in cells loaded with ^{ROX}SA at doses up to 50 μM after 48 h culturing (Figure S6, Supporting Information). These advantageous characters are beneficial for continual fluorescence tracking with ^{ROX}SA.

Imaging of Mitophagic Cells with ^{ROX}SA. Given the causal roles of mitophagy in multiple diseases,[6] we first examined the performance of ^{ROX}SA in long-term tracking lysosomes in mitophagy. U2OS cells were stained with ^{ROX}SA and LysoTracker Red and then starved in DMEM depleting serum to induce mitophagy. Lysosomal pH increases in autophagic cells upon fusion of acidic lysosomes with neutral autophagosomes. Intense fluorescence of ^{ROX}SA was present in cells after 24 h starvation whereby LysoTracker Red is largely diminished (Figure 3 and Figure S7, Supporting Information), showing the use of ^{ROX}SA to track stressed lysosomes in mitophagy.

Based on these results, we carried on a whole course of imaging of mitophagy using cells co-stained with ^{ROX}SA and MitoTracker Green which covalently labels mitochondria and

DOI: 10.1021/acs.analchem.8b02365
Anal. Chem. 2018, 90, 11393−11400

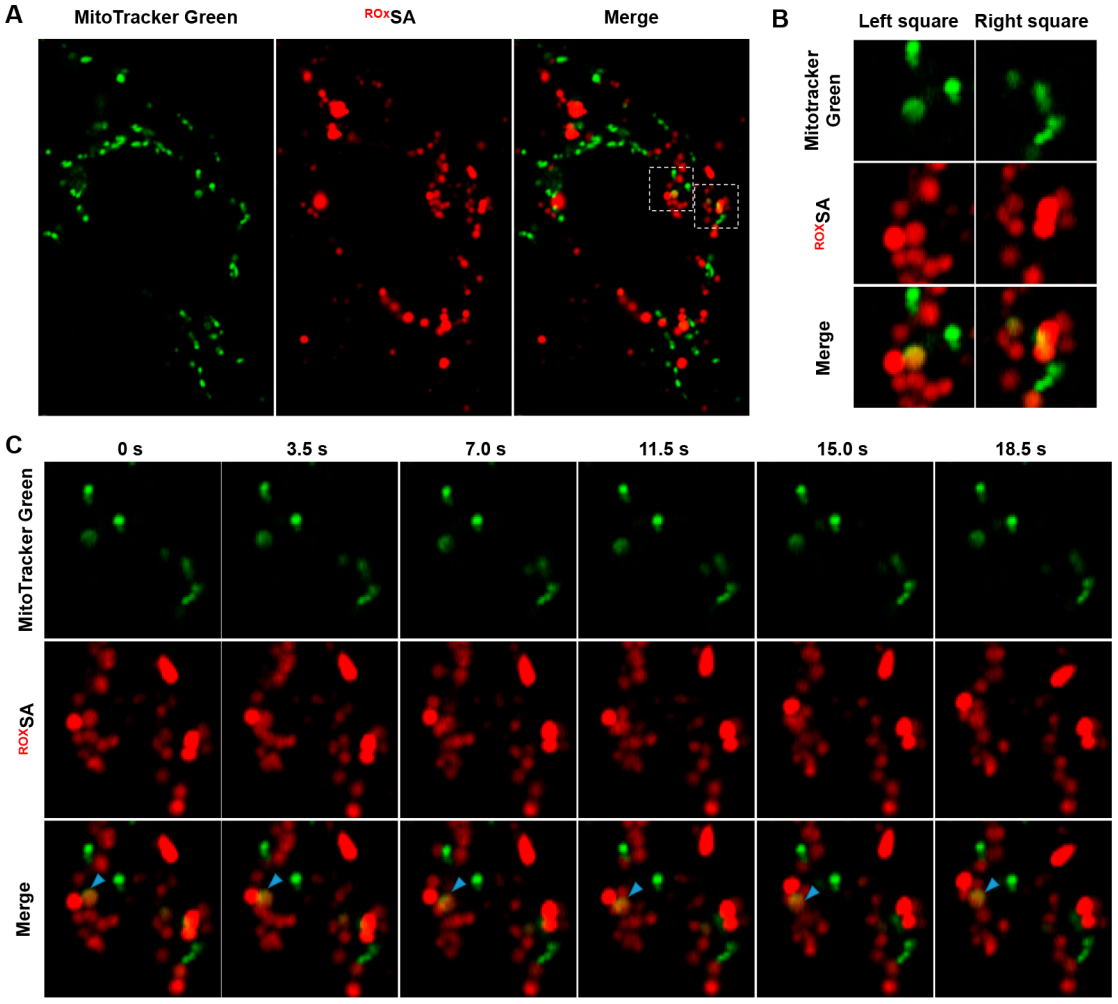

Figure 4. Imaging of lysosome−mitochondrion interplay in mitophagy with ^{ROX}SA. U2OS cells stained with ^{ROX}SA and MitoTracker Green were starved to induce mitophagy. (A) Confocal microscopic images of mitophagic cells at 24 h post-starvation. (B) Zoomed images of the indicated areas. (C) Snapshots of a mitochondrion encapsulated in a lysosome. Colocalization of MitoTracker Green with ^{ROX}SA is indicated by arrowheads. Scale bar, 10 μm.

allows tracking of mitochondria. Confocal microscopy revealed consumption of lysosomes into less and larger lysosomes in cells at 24−48 h post-starvation and restoration of lysosome size to normal states at 72−120 h after starvation (Figure 3A). In parallel, LysoTracker-based staining confirmed that all the lysososmes are ^{ROX}SA-positive in the whole course of mitophagy (Figure S8, Supporting Information). These observations are consistent with reported fusion of multiple lysosomes with autophagosome to form larger autolysosomes and subsequent re-formation of lysosomes from autolysosomes.[23] Consecutive snapshots recorded over a 335−525 s time period at 24 h after starvation showed the approach, contact, and fusion of two individual lysosomes (Figure 3B). Furthermore, confocal microscopy clearly revealed two distinct states of mitochondria that are physically apart from or encapsulated in lysosomes (Figure 4A,B). The mitophagy was further confirmed by time course studies, which showed constant colocalization of MitoTracker Green with ^{ROX}SA over time (Figure 4C). Collectively, these data validate the utility of ^{ROX}SA to track dynamic lysosomes and mitochondrial−lysosomal interactions in live cells.

Super-resolution Imaging of Lysosomes with ^{ROX}SA. Super-resolution imaging is of enormous use in investigating cell events.[9] Recent advances in super-resolution microscopy, such as stochastic optical reconstruction microscopy (STORM), have broken the diffraction limit of conventional light microscopy and allowed resolution down to ∼10 nm to be achieved.[8] Photoswitchable fluorophores are required for single-molecule localization microscopy. Since rhodamines could be converted between fluorescence-on and dark states multiple times upon light excitation,[24] we evaluated the compatibility of ^{ROX}SA to high-resolution STORM imaging. Albeit both dyes were blinking under high laser illumination, we observed high-quality images of lysosomes stained with ^{ROX}SA over LysoTracker Red (Figure 5A,B). Consistently the number of ^{ROX}SA molecules in individual lysosomes was identified to be much higher than that of LysoTracker Red (399.2 ± 36.6 vs 142.6 ± 14.1; Figure 5C). Moreover, ^{ROX}SA exhibited higher photon yields than LysoTracker Red (Figure 5 D), resulting in enhanced localization accuracy and high-resolution lysosomal images (Figure 5A,B). Relative to LysoTracker Red, ^{ROX}SA, with superior photostability and pH-independent lysosomal retention, is an ideal lysosome-illuminating probe with high localization accuracy beneficial for super-resolution microscopy. Given the resolution of superimaging to ∼10 nm, the demonstrated attributes of ^{ROX}SA support its potential to

DOI: 10.1021/acs.analchem.8b02365
Anal. Chem. 2018, 90, 11393−11400

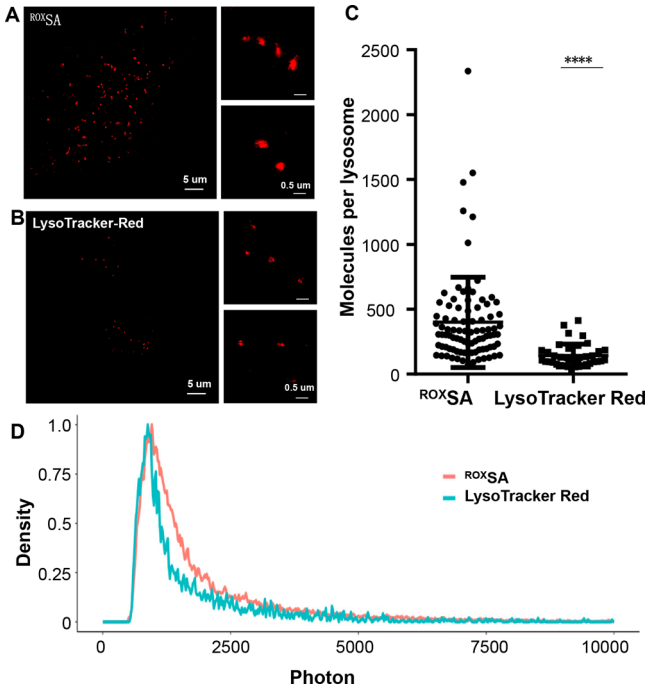

Figure 5. Super-resolution STORM imaging of lysosomes with ^{ROX}SA. STORM images of HeLa cells stained with ^{ROX}SA (A) or LysoTracker Red (B). Scale bars: 5 or 0.5 μm as indicated. (C) Identified molecules per lysosome of HeLa cells loaded with ^{ROX}SA or LysoTracker Red. Results shown are mean ± sem. ****, $P < 0.0001$. (D) Distribution of number of photons detected for individual ^{ROX}SA or LysoTracker Red.

investigate vesicles smaller than lysosomes, such as budding vesicles from lysosomes.

CONCLUSIONS

Stressed lysosomes are manifested in myriad diseases and are often challenging to visualize with acidotropic dyes. To overcome the liability of acidotropic dyes to escape lysosomes, we herein report an alternative and simplified approach to track lysosomes using ^{ROX}SA. Stably maintained in lysosomes without resort to lysosomal acidity, ^{ROX}SA exhibits high photostability and long-term retention in lysosomes and is compatible with STORM super-resolution imaging, which enables whole course spatiotemporal tracking of lysosomes and lysosome−mitochondrial interaction in mitophagy. Several strategies have been developed to track stressed lysosomes,[25] such as the cell-penetrating, peptide-conjugated suicide substrate of Cathesin B. Albeit powerful, these approaches necessitate rather complex synthetic probes. With the distinct lysosome-residing mechanism from conventional LysoTrackers, ^{ROX}SA offers a robust and simplified optical tool for investigating lysosome biology.

ASSOCIATED CONTENT

Supporting Information

The Supporting Information is available free of charge on the ACS Publications website at DOI: 10.1021/acs.analchem.8b02365.

Figures of cell uptake of ROX and 5-ROX, uptake of ^{ROX}SA by distinct cell lines, pH titration of ^{ROX}SA, mechanisms on cell uptake of ^{ROX}SA, and comparison of mitophagy imaging using ^{ROX}SA over LysoTrackers (PDF)

AUTHOR INFORMATION

Corresponding Authors

*(S.H.) E-mail: shoufa@xmu.edu.cn. Fax: +865922181728.
*(X.C.) E-mail: threegold@xmu.edu.cn Fax: +865922181728.

ORCID

Shoufa Han: 0000-0003-3389-9318

Notes

The authors declare no competing financial interest.

ACKNOWLEDGMENTS

This work was supported by grants from NSF China (21775130 and 21572189) and the Fundamental Research Funds for the Central Universities (207201 60052, and 20720150047), Xiamen University; J.H. was supported by grants from NSF China (91429301, 31420103910, and 31330047), the National Scientific and Technological Major Project (2013ZX10002-002), and the Hi-Tech Research and Development Program of China (863program; 2012AA02A201); and X.C. was supported by a grant from NSF China (31501115).

REFERENCES

(1) (a) Baixauli, F.; Acin-Perez, R.; Villarroya-Beltri, C.; Mazzeo, C.; Nunez-Andrade, N.; Gabande-Rodriguez, E.; Ledesma, M. D.; Blazquez, A.; Martin, M. A.; Falcon-Perez, J. M.; Redondo, J. M.; Enriquez, J. A.; Mittelbrunn, M. *Cell Metab.* **2015**, *22* (3), 485−98. (b) Tait, S. W.; Green, D. R. *Nat. Rev. Mol. Cell Biol.* **2010**, *11* (9), 621−32. (c) Repnik, U.; Turk, B. *Mitochondrion* **2010**, *10* (6), 662−9. (d) Kroemer, G.; Jaattela, M. *Nat. Rev. Cancer* **2005**, *5* (11), 886−97.

(2) (a) Lim, C. Y.; Zoncu, R. *J. Cell Biol.* **2016**, *214* (6), 653−64. (b) Stinchcombe, J.; Bossi, G.; Griffiths, G. M. *Science* **2004**, *305* (5680), 55−9.

(3) Settembre, C.; Fraldi, A.; Medina, D. L.; Ballabio, A. *Nat. Rev. Mol. Cell Biol.* **2013**, *14* (5), 283−96.

(4) Kogot-Levin, A.; Zeigler, M.; Ornoy, A.; Bach, G. *Pediatr. Res.* **2009**, *65* (6), 686−90.

(5) Fehrenbacher, N.; Jaattela, M. *Cancer Res.* **2005**, *65* (8), 2993−5.

(6) (a) Bravo-San Pedro, J. M.; Kroemer, G.; Galluzzi, L. *Circ. Res.* **2017**, *120* (11), 1812−1824. (b) Von Stockum, S.; Nardin, A.; Schrepfer, E.; Ziviani, E. *Neurobiol. Dis.* **2016**, *90*, 58−67. (c) Kerr, J. S.; Adriaanse, B. A.; Greig, N. H.; Mattson, M. P.; Cader, M. Z.; Bohr, V. A.; Fang, E. F. *Trends Neurosci.* **2017**, *40* (3), 151−166.

(7) (a) Xue, Z.; Zhao, H.; Liu, J.; Han, J.; Han, S. *ACS Sens* **2017**, *2* (3), 436−42. (b) Li, Z.; Wu, S.; Han, J.; Han, S. *Analyst* **2011**, *136* (18), 3698−706. (c) Wan, Q.; Chen, S.; Shi, W.; Li, L.; Ma, H. *Angew. Chem., Int. Ed.* **2014**, *53* (41), 10916−20. (d) Li, G.; Zhu, D.; Xue, L.; Jiang, H. *Org. Lett.* **2013**, *15* (19), 5020−3. (e) Dong, B.; Song, X.; Wang, C.; Kong, X.; Tang, Y.; Lin, W. *Anal. Chem.* **2016**, *88* (7), 4085−91. (f) Wang, Q.; Zhou, L.; Qiu, L.; Lu, D.; Wu, Y.; Zhang, X. B. *Analyst* **2015**, *140* (16), 5563−9.

(8) (a) Doksani, Y.; Wu, J. Y.; de Lange, T.; Zhuang, X. *Cell* **2013**, *155* (2), 345−356. (b) Xu, K.; Zhong, G.; Zhuang, X. *Science* **2013**, *339* (6118), 452−6.

(9) Huang, B.; Babcock, H.; Zhuang, X. *Cell* **2010**, *143* (7), 1047−58.

(10) Pierzynska-Mach, A.; Janowski, P. A.; Dobrucki, J. W. *Cytometry, Part A* **2014**, *85* (8), 729−37.

(11) Li, C.; Evans, R. M. *Nucleic Acids Res.* **1997**, *25* (20), 4165−6.

(12) Vaughan, J. C.; Jia, S.; Zhuang, X. *Nat. Methods* **2012**, *9* (12), 1181−4.

(13) (a) Verheijen, F. W.; Verbeek, E.; Aula, N.; Beerens, C. E.; Havelaar, A. C.; Joosse, M.; Peltonen, L.; Aula, P.; Galjaard, H.; van der Spek, P. J.; Mancini, G. M. *Nat. Genet.* **1999**, *23* (4), 462−5. (b) Aula, P.; Autio, S.; Raivio, K. O.; Rapola, J.; Thoden, C.-J.; Koskela, S.-L.; Yamashina, I. *Arch. Neurol.* **1979**, *36* (2), 88−94. (c) Renlund, M.; Aula, P.; Raivio, K. O.; Autio, S.; Sainio, K.; Rapola, J.; Koskela, S. L. *Neurology* **1983**, *33* (1), 57−66.

DOI: 10.1021/acs.analchem.8b02365
Anal. Chem. 2018, 90, 11393−11400

(14) (a) Han, S.; Collins, B. E.; Bengtson, P.; Paulson, J. C. *Nat. Chem. Biol.* **2005**, *1* (2), 93−7. (b) Lin, B.; Wu, X.; Zhao, H.; Tian, Y.; Han, J.; Liu, J.; Han, S. *Chem. Sci.* **2016**, *7*, 3737. (c) Luchansky, S. J.; Goon, S.; Bertozzi, C. R. *ChemBioChem* **2004**, *5* (3), 371−4. (d) Sampathkumar, S. G.; Li, A. V.; Jones, M. B.; Sun, Z.; Yarema, K. J. *Nat. Chem. Biol.* **2006**, *2* (3), 149−52. (e) Sun, Y.; Hong, S.; Xie, R.; Huang, R.; Lei, R.; Cheng, B.; Sun, D. E.; Du, Y.; Nycholat, C. M.; Paulson, J. C.; Chen, X. *J. Am. Chem. Soc.* **2018**, *140* (10), 3592−3602.

(15) (a) Zhang, S.; Chen, T. H.; Lee, H. M.; Bi, J.; Ghosh, A.; Fang, M.; Qian, Z.; Xie, F.; Ainsley, J.; Christov, C.; Luo, F. T.; Zhao, F.; Liu, H. *ACS Sens* **2017**, *2* (7), 924−931. (b) Wu, X.; Yu, M.; Lin, B.; Xing, H.; Han, J.; Han, S. *Chem. Sci.* **2015**, *6* (1), 798−803.

(16) Yoshimori, T.; Yamamoto, A.; Moriyama, Y.; Futai, M.; Tashiro, Y. *J. Biol. Chem.* **1991**, *266* (26), 17707−12.

(17) Schultz, K. R.; Gilman, A. L. *Leuk. Lymphoma* **1997**, *24* (3−4), 201−10.

(18) Nakase, I.; Niwa, M.; Takeuchi, T.; Sonomura, K.; Kawabata, N.; Koike, Y.; Takehashi, M.; Tanaka, S.; Ueda, K.; Simpson, J. C.; Jones, A. T.; Sugiura, Y.; Futaki, S. *Mol. Ther.* **2004**, *10* (6), 1011−22.

(19) Inal, J.; Miot, S.; Schifferli, J. A. *Exp. Cell Res.* **2005**, *310* (1), 54−65.

(20) (a) Smart, E. J.; Anderson, R. G. *Methods Enzymol.* **2002**, *353*, 131−9. (b) Ros-Baro, A.; Lopez-Iglesias, C.; Peiro, S.; Bellido, D.; Palacin, M.; Zorzano, A.; Camps, M. *Proc. Natl. Acad. Sci. U. S. A.* **2001**, *98* (21), 12050−5.

(21) (a) Harding, E. A.; Day, M. L.; Gibb, C. A.; Johnson, M. H.; Cook, D. I. *Pfluegers Arch.* **1999**, *438* (3), 397−404. (b) Christensen, K. A.; Myers, J. T.; Swanson, J. A. *J. Cell Sci.* **2002**, *115* (3), 599−607.

(22) Lin, B.; Wu, X.; Zhao, H.; Tian, Y.; Han, J.; Liu, J.; Han, S. *Chem. Sci.* **2016**, *7*, 3737−41.

(23) Yu, L.; McPhee, C. K.; Zheng, L.; Mardones, G. A.; Rong, Y.; Peng, J.; Mi, N.; Zhao, Y.; Liu, Z.; Wan, F.; Hailey, D. W.; Oorschot, V.; Klumperman, J.; Baehrecke, E. H.; Lenardo, M. J. *Nature* **2010**, *465* (7300), 942−6.

(24) Folling, J.; Belov, V.; Kunetsky, R.; Medda, R.; Schonle, A.; Egner, A.; Eggeling, C.; Bossi, M.; Hell, S. W. *Angew. Chem., Int. Ed.* **2007**, *46* (33), 6266−70.

(25) (a) Hu, F.; Cai, X.; Manghnani, P. N.; Kenry; Wu, W.; Liu, B. *Chem. Sci.* **2018**, *9*, 2756−61. (b) Leung, C. W.; Wang, Z.; Zhao, E.; Hong, Y.; Chen, S.; Kwok, R. T.; Leung, A. C.; Wen, R.; Li, B.; Lam, J. W.; Tang, B. Z. *Adv. Healthcare Mater.* **2016**, *5* (4), 427−31. (c) Han, Y.; Li, M.; Qiu, F.; Zhang, M.; Zhang, Y. H. *Nat. Commun.* **2017**, *8* (1), 1307. (d) Xue, Z.; Zhang, E.; Liu, J.; Han, J.; Han, S. *Angew. Chem., Int. Ed.* **2018**, *57*, 10096.

DOI: 10.1021/acs.analchem.8b02365
Anal. Chem. 2018, 90, 11393−11400